Modeling nonclassical nonlinearity, conditioning, and slow dynamics effects in mesoscopic elastic materials

P. P. Delsanto and M. Scalerandi
INFM - Dip. Fisica, Politecnico di Torino, C.so Duca degli Abruzzi 24, 10129, Torino, Italy
(Received 2 January 2003; published 12 August 2003)

Several materials with mesoscopic characteristics (e.g., defects or intergrain regions) have been shown to share several nonclassical nonlinear features, which distinguish them from classical nonlinear media. Most striking among them is the log-time recovery of the material properties after they have been conditioned by the action of an external perturbation. A simple model based on the description of the mesoscopic features as bond regions between elastic portions is presented here. The implementation of the model is illustrated by the application of a special bi-state protocol, which, by considering also thermally induced transitions between the two basic states, allows to explain all experimentally observed nonclassical nonlinear effects.

DOI: 10.1103/PhysRevB.68.064107 PACS number(s): 62.30.+d, 91.60.−x, 02.70.−c

I. INTRODUCTION

A tremendous amount of research work has been carried on in recent years in the field of Molecular Dynamics,[1] including *ab initio* calculations, pseudopotential energy approaches, atomistic models, etc. At the same time, the development of more and more sophisticated industrial processes and products, in all fields of applications, requires a correspondingly large progress in the understanding of the materials employed, their basic properties and behavior under changes of environmental conditions, components interactions, etc. A deeper understanding of materials must, of course, be related to what one learns about their microscopic structure and dynamics. Yet, bridging from a microscopic to a macroscopic description of matter is extremely difficult, since, after all, there is a gap spanning about ten orders of magnitude between the two scales. As a consequence, in spite of the huge progress in both, very little information percolates from the former to the latter.

Modeling and numerical simulations at the mesoscopic level[2,3] offer a natural and powerful approach to the solution of the problem discussed above, i.e., exploiting the advances of molecular dynamics for applications in nondestructive evaluation, material science, seismic studies, and engineering. In fact, the discretization of a material specimen in a lattice of, say, $500\times500\times500$ grid elements (cells) allows for the possibility of considering at the local level features of the order of a micrometer. At that size it becomes possible to analyze and implement local mechanisms, which should eventually be inferred, e.g., by atomistic models.

Of particular interest within this context is the numerical simulation of both quasistatic and resonant dynamic experiments, which have been performed in recent years[4–6] on a variety of materials, such as rocks, soil, damaged and intact concretes, metal alloys with mesoscopic flaws, etc. In spite of their very different microstructure and chemistry, all these materials exhibit the same peculiar elastic nonlinear behavior, which we shall call nonclassical, since it cannot be explained by the classical nonlinear theory of Landau.[7,8]

The quasistatic experiments reveal the existence of an hysteretic loop in the stress-strain relation with end-point memory.[9] Phase shifts in resonance experiments, the generation of higher-order harmonics with a well-defined rate, nonclassical attenuation, and other effects have also been found.[5] Perhaps the most striking feature observed so far is the so-called ''slow dynamics,'' which consists in a downshift of the resonance frequency when the specimen has been dynamically excited, and consequent recovery proportional to the logarithm of the elapsed time.[10,11]

It is remarkable that ''fast dynamics'' effects are always accompanied by ''slow dynamics'' effects and vice versa.[12] The former are direct results of mesoscopic features (grain structures, interstices, cracks, etc.), while the latter depend directly on atomic/molecular mechanisms (from which, of course, also the former ultimately derive). The two kinds of effects are very well separated in terms of times involved (fraction of seconds vs minutes or even hours, days) and no effects on other scales have been observed.

The results of quasistatic[13,14] and ''fast dynamics''[15,16] have been well reproduced by the models based on the Local Interaction Simulation Approach (LISA),[17] applied in conjunction with a Spring Model[18] and a Preisech-Mayergoitz (PM) representation.[19,20] In these models the specimen is described as a sequence of elastic elements, the ''grains,'' and nonclassical regions corresponding to the interstices (called Hysteretic Mesoscopic Units—HMU), which behave either rigidly or elastically, depending on the local pressure.[15]

The purpose of the present contribution is to include the basic ingredients previously proposed[14,15] into a more general and flexible model, which should provide a suitable vehicle for the introduction of realistic (i.e., based on physical considerations), rather than phenomenological interaction forces. In addition, the model, by including thermally activated random transitions between different intersticial states, allows one to keep into account the stress history of the specimen. It becomes then possible to predict effects, such as the specimen conditioning and logarithmic recovery, which are ''signatures'' of slow dynamics and, to our knowledge, have not yet been predicted by other models.

The proposed model is presented in the following section. The protocol, i.e., the set of initial and boundary conditions

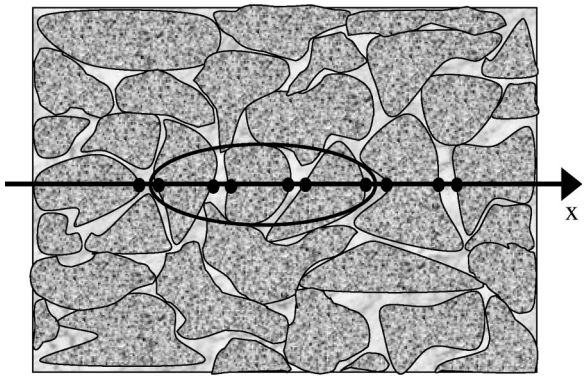

FIG. 1. 2D representation of a multigrained material specimen.

and detailed specifications of the behavior of the HMU's, which we have adopted in order to implement the model in numerical simulations, is described in Sec. III. In Sec. IV, the problem of wave propagation in a bar made of a multigrained material is defined (and the relevant parameters are specified). Both ''fast'' and ''slow'' dynamics effects are then simulated, with an excellent qualitative agreement with available experimental results.

II. THE MODEL

A. Specimen discretization

The problem we wish to analyze is the propagation of an ultrasonic wave through a multigrained material specimen (see Fig. 1). If the specimen consists of a thin bar, we can simplify the problem with a one-dimensional (1D) schematization in which longer segments representing grains alternate with shorter ones representing interstices (see Fig. 2).

Following the Spring Model of Ref. 18, the representation of Fig. 2 corresponds to a lattice in which each node i is split into two subnodes i^- and i^+, delimiting the ith interstice ($i=1,I-1$, where I is the total number of grains included in the discretization of the bar). We shall label with the same index i also the grain to the left of the interstice and call l_i its length. We also assign to each subnode $i^\pm$ the mass $m_i^\pm$ of half of the grain to the right and left of the subnode, respectively. If the density ρ is constant, we have $m_i^- = 1/2\rho l_i$, $m_i^+ = 1/2\rho l_{i+1}$. An advantage of the Spring Model representation is the natural way in which the formalism can be extended to 2D and 3D.[21]

B. Constitutive relationships

Both in the grains and in the interstices we consider forces (or stresses) acting on the subnodes, which we shall call $F_i^\pm$ and $f_i^\pm$, respectively, as depicted in Fig. 2. Neglecting temperature effects (i.e., assuming the temperature to be constant), the forces $F_i^\pm$ depend on the strain ε_i of the grain, while the intersticial forces $f_i^\pm$ have, in general, a more complex dependence on external factors. In fact, since interstices may be thought of as bonding regions among grains, $f_i^\pm$ represent the reaction of the bond to the incoming disturbance. They also include implicitely the effects of the surrounding grains.

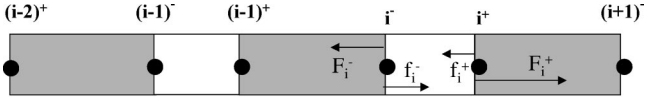

FIG. 2. 1D schematization: gray areas represent the grains and white areas the interstices.

The explicit expression of $f_i^\pm$ should be evinced from a detailed knowledge of interaction mechanisms at the molecular or mesoscopic level, e.g., dislocations theory,[22] the Biot theory for capillary pressure,[23] glass transitions,[24] etc. Since such information is not yet available, we limit ourselves to a phenomenological treatment, in which $f_i^\pm$ is assumed to depend on the propagating external pressure and on the interstice strain η (or deformation δ) and its first time derivative:

$$f = f^+ = -f^- = f(P, \delta, \dot{\delta}), \tag{1}$$

where

$$P = F^- - F^+,$$

$$\delta = u^+ - u^-. \tag{2}$$

Here and in the following the node index is omitted for brevity when equal to i. $u^\pm$ are the displacements of the two subnodes $i^\pm$. $f^- = -f^+$ since the interstice is assumed to be massless. Forces (both $F^\pm$ and $f^\pm$) are considered to be positive when pointing to the right, while pressure and strains are defined to be positive when compressional.

By assuming, as a first step, that both the grain and interstice forces may be approximated as linear, we obtain the constitutive relationships

$$F^\pm = \pm K\varepsilon^\pm, \tag{3}$$

and

$$f = a_1 P + a_2 \delta + a_3 \dot{\delta}, \tag{4}$$

where K is the (linear) elastic constant of the grain, $\varepsilon^- = \varepsilon_i$, $\varepsilon^+ = \varepsilon_{i+1}$, and $a_n (n=1,2,3)$ are the linear expansion coefficients.

Nonlinear terms can (and should) be added to both Eqs. (3) and (4). Since, however, we are mostly interested, in the present context, in nonclassical nonlinearities, we neglect them entirely in Eq. (3) and explicitely in Eq. (4), i.e., we assume that a_n may depend on P, while K may not. More precisely, we assume that the interstice is normally in a ''linear'' state (a_n constant), except for a number of sudden transitions from a linear state to another, due, e.g., to local modifications induced by the propagating disturbance. We call ''protocol'' the explicit dependence $a_n(P)$, including the initial conditions. Although, in principle, a detailed specification of $a_n(P)$ is necessary for a detailed prediction of the behavior of the interstice, in practice, at a macroscopic level, the large number of interstices (usually many 1000's) dilutes the relevance of the particular protocol for any of them. Thus, as we will see later, even a very simple protocol suf-

fices to reproduce all the observed phenomena in quasistatic[14] and dynamic resonant experiments (see Sec. IV).

A basic feature that must be included in any protocol is the natural ''resistance'' of the grains surface and interstitial matter in returning to the initial state when the pressure is released. This leads to a different $a_n(P)$ dependence when P decreases and, as a consequence, to hysteretic loops. Another important feature to be added to the protocol is the possibility, due to thermal activation, of random transitions between the two branches of $a_n(P)$.

C. Equations of motion

From the constitutive laws, the equations of motion for the two subnodes $i^{\pm}$ easily follow

$$m^{\pm}\ddot{u}^{\pm}=F^{\pm}\pm f-\gamma\dot{u}^{\pm}, \tag{5}$$

where an attenuative term with coefficient γ has been included.

Since, due to the large number of HMU's, the details of the specimen discretization are unimportant, we can assume for simplicity that $l^{+}=l^{-}=l$. By applying the usual first-order finite difference formalism and assuming, for the sake of notational simplicty that the time step $\tau=1$, we obtain

$$\delta(t+1)=\frac{1}{m-\alpha}[(2a_1-1)P+2(m+a_2)\delta(t) -(m+\alpha)\delta(t-1)], \tag{6}$$

$$y(t+1)=\frac{1}{2m+\gamma}[F^{+}+F^{-}+4my(t)-(2m-\gamma)y(t-1)], \tag{7}$$

where

$$\alpha=a_3-\frac{\gamma}{2},$$

and

$$y=\frac{1}{2}(u^{+}+u^{-})$$

represents the displacement of the interstice center of mass. From the definitions of y and δ, the corresponding equations for u^{+} and u^{-} can be easily obtained.

III. THE PROTOCOL

A. Bi-state protocol

Assuming, as discussed in Sec. II B, to consider only linear intersticial states and sudden nonlinear transitions from one to the next, the detailed information about the parameters of each state and each transition, including the values of the pressure at which they occur, should be evinced from basic physical considerations. In principle, we could expect to have, for each HMU, a long ''ladder'' of transitions vs P, with a different return path, giving rise to a hysteretic loop.

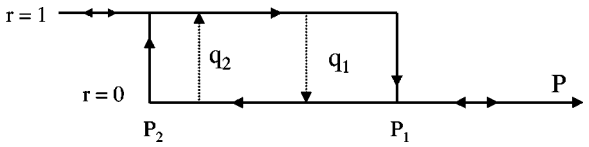

FIG. 3. Basic hysteretic loop for each HMU. We assume that $r=1$ represents a ''free'' state and $r=0$ a ''rigid'' one. q_1 and q_2 are the thermal activated transition rates between the two states.

Since, however, the very large number of HMU's washes away the relevance of a detailed description, we replace for each HMU the ladder with a basic bi-state ''block'' (see Fig. 3), in which two linear states coexist in the pressure range (P_1,P_2). The two states represent the interstice behavior when the pressure is increased or, respectively, decreased and are labeled by the two arbitrary values of the state variable r (e.g., $r=0$ and $r=1$).

In addition to the hysteretic behavior, Fig. 3 shows the thermal activated random transition rates q_1 and q_2 between the two linear states. These states may be assumed to be both ''free,'' i.e., with δ elastically variable, or both ''rigid,'' i.e., with δ bound not to change thereafter, or one free and one rigid. The two former choices may be aesthetically more pleasant, due to their symmetry. We adopt, however, the latter choice (a free and a rigid state), since a free state is more intuitively physical, but a rigid state helps in explaining the experimental observation of residual strains at $P=0$ in quasistatic compressional experiments.[14] In fact, residual strains at zero stress, which disappear very slowly with time, imply the (at least temporary) existence of interstice configurations, reached during phases of increasing pressure, which remain ''frozen'' during pressure release.

The protocol is then defined as follows (see Fig. 3). Starting for any given HMU at a given pressure $P<P_1$, we assume that δ varies elastically $(r=1)$ up to $P=P_1$, at which point it becomes rigid (r drops to 0). Conversely, when P decreases, the HMU remains rigid up to the value $P=P_2$, where r jumps to 1 and the HMU becomes elastic again. Since the rigid state $(r=0)$ is expected to be more stable than the elastic one, we assume for the thermal activated transition rates that $q_1>q_2$. These hopping transition rates increase, of course, with the temperature, but in the present context, in which only isothermal processes are considered, this dependence is not explicitly included. Likewise, any other dependence of the rates on, e.g., the applied pressure P is neglected.

The choice of the set of pairs of parameters (P_1,P_2) for each HMU is, of course, crucial for the performance of any given protocol. Such a set is usually represented in the so-called PM space, i.e., as a distribution of points in a (P_1,P_2) plane. In the case of virtual quasistatic experiments, in which pressures up to 10^8 Pa are involved, the PM space distribution is obtained by inverting the experimental data.[13,25] For the simulation of resonant dynamic experiments the range of pressures is usually much smaller and only an extremely small portion of the PM space around the ambient pressure P_o is explored by the incoming perturbation. In such a tiny region, it is reasonable to assume a uniform distribution of (P_1,P_2) points.

As a result of the proposed protocol and convention ($r=0,1$), we rewrite Eq. (6) as follows:

$$\delta(t+1)=\delta(t)+r[b_1P+b_2\delta(t)-b_3\delta(t-1)], \qquad (8)$$

where b_n are the coefficients in the elastic case ($r=1$),

$$b_1=\frac{2a_1-1}{m-\alpha},$$

$$b_2=\frac{m+\alpha+2a_2}{m-\alpha}, \qquad (9)$$

$$b_3=\frac{m+\alpha}{m-\alpha}.$$

B. Initial and boundary conditions

We assume that at the beginning (i.e., before starting the ''virtual experiment'') the specimen is completely relaxed and kept at the atmospheric pressure P_o. For simplicity, we redefine the pressure scale, so that $P_o=0$. Three cases are possible (see Fig. 3).

(1) $P_2>0$, then only the state $r=1$ is allowed;

(2) $P_1<0$, then only the state $r=0$ is possible;

(3) $P_2<0<P_1$, then both states are allowed.

Since the specimen is relaxed, the state distribution is in equilibrium condition. Hence their respective probabilities are given by

$$p(r=1)=1-p(r=0)=\frac{q_2}{q_1+q_2}. \qquad (10)$$

In a dynamic experiment, the boundary conditions are given by an external forcing [e.g., $F=F_0\cos(\omega t)$ for a monochromatic wave] at one end of the bar and free boundary conditions (zero stress) at the other.

C. Predictions of the Young modulus behavior

It may be useful to visualize the discretized bar as composed of units including both a grain and a HMU [e.g., from $(i-1)^+$ to i^+ in Fig. 2]. Its effective elastic constant K_i may then be obtained from the elastic constants of the grain K and of the HMU $K'=-2a_2/(1+2a_1)$:

$$\frac{1}{K_i}=\frac{1}{K}+\frac{1}{K'}. \qquad (11)$$

Note that K' varies with time and space and so does K_i. At any given time T, the bar Young modulus is then given by

$$\frac{1}{Y}=\frac{1}{I}\sum_{i=1}^{I}\frac{1}{K_i}=\frac{1}{K}+\frac{N_e}{K'},$$

where N_e is the number of HMU's, which, at $t=T$, are in the elastic state (the other ones do not contribute, since they are rigid). N_e depends, of course, on the local pressure distribution (hence on the driving excitation amplitude), but also on the stress history of the specimen.

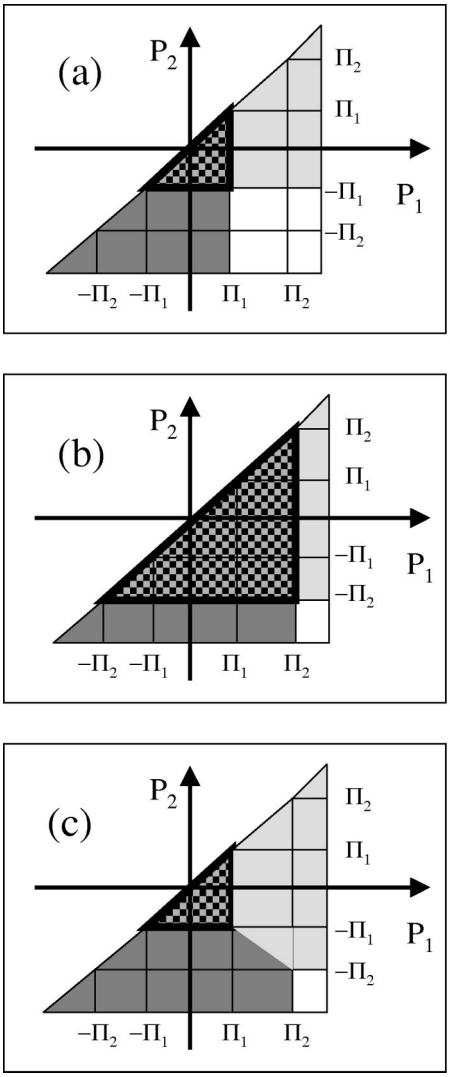

FIG. 4. Distributuion of HMU's according to their elastic properties: permanently elastic (light gray areas), permanently rigid (dark gray areas), variable between the two cases (checkered areas), frozen in their initial condition (white area). (a) Pressure range $-\Pi_1<P<\Pi_1$, (b) range $-\Pi_2<P<\Pi_2$ with $\Pi_1<\Pi_2$, (c) sudden return to the $-\Pi_1<P<\Pi_1$ range.

Let us now consider a dynamic experiment and assume, at first, that the local pressure varies between $-\Pi_1$ and Π_1 $(-\Pi_1<P<\Pi_1)$. Neglecting the effects of thermal activation transitions (which become important on a much longer time scale than that of dynamic experiments), we find the following possibilities, according to the location of (P_1,P_2) in the PM space [see Fig. 4(a)].

(1) In the region $P_1>\Pi_1, P_2>-\Pi_1$ (light gray area), the HMU's are permanently elastic.

(2) In the region $P_1<\Pi_1, P_2<-\Pi_1$ (dark gray area), the HMU's are permanently rigid;

(3) In the region $-\Pi_1<P_1, P_2<\Pi_1$ (checkered area), the HMU's are switching twice for each cycle between the two states. Their contribution to the elastic constant is proportional to the occupancy rate of the $r=1$ state.

(4) In the region $P_1>\Pi_1, P_2<-\Pi_1$ (white area), the HMU's remain in their inital state.

Increasing the driving amplitude, the local pressure excursion increases [see Fig. 4(b)] to $-\Pi_2<P<\Pi_2$. As a consequence, the HMU's elastic properties change as depicted. Due to symmetry considerations, the changes in the HMU's, whose elastic state becomes variable with time ($\Pi_1<P_1<\Pi_2; -\Pi_2<P_2$ and $-\Pi_2<P_2<-\Pi_1; P_1<\Pi_1$) mutually compensate. This is not true for the other affected regions ($\Pi_1<P_1<\Pi_2; P_2<-\Pi_2$ and $-\Pi_1<P_2<-\Pi_2; P_1>\Pi_2$), since in the initial distribution rigid units are dominant ($q_1>q_2$) with respect to the elastic ones. As a consequence, a softening effect will appear, as experimentally observed.

Let us now suppose to reduce the specimen excitation to the previous lower amplitude Π_1, without allowing time for relaxation. The corresponding distribution in the PM space is depicted in Fig. 4(c). Not all the HMU's go back to the same configuration as in Fig. 4(a) and the specimen elastic modulus remains approximately the same as at the larger amplitude Π_2. Note that the state of units in the region $\Pi_1<P_1<\Pi_2; -\Pi_1<P_2<-\Pi_2$ strongly depends on the pressure behavior during the transition to the low amplitude excitation and cannot be predicted *a priori*.

From the configuration of Fig. 4(c), after a sufficiently long time, relaxation occurs. In fact, in the region $P_1>\Pi_1; P_2<-\Pi_1$, the pressure is constantly in the interval (P_1,P_2). As a consequence, random transitions slowly lead towards a stationary configuration as in Fig. 4(a).

IV. RESULTS AND DISCUSSION

In order to illustrate the applicability of the model and protocol discussed in the previous sections, we present in the following a few numerical examples. The parameters chosen for the reported simulations (expressed for generality in arbitrary units) are $I=1000$, $K=1$, $a_1=0.99$, $a_2=3$ (unless otherwise specified), $a_3=1$, $\rho=1$, $\gamma=0.001$, $q_1=0.0003$, and $q_2=0.0001$. The opening and closing pressures for the HMU's have been chosen in the range $[-0.1,0.1]$.

Since quasistatic ''in-silico'' experiments have been discussed elsewhere,[14] we limit ourselves here to simulate dynamic resonant experiments. We assume that monochromatic waves of driving amplitude F_0 and varying frequency ω are input in a rod-shaped specimen by a transducer attached to one end of the specimen. The signal is recorded by an accelerometer attached to the other end. At any given excitation level, the frequency ω is swept through the fundamental resonance mode ω_R of the specimen and the time-averaged acceleration amplitude A (in stationary conditions) is recorded. This procedure of resonance curve tracking is repeated for several different levels of excitation.

In the course of the experiments several macroscopic effects can be observed, resulting from the proposed microscopic interaction mechanisms, as discussed in Sec. III C.

(1) ''Mechanical'' interactions induce variations in the effective elastic moduli of the HMU's, which are directly perturbed by the external excitation. As a result a resonance frequency shift is observed.

(2) Stress-history effects are also induced, leading to variations in the dynamic moduli that do not immediately disappear when the disturbance is removed. In other words, the specimen is ''conditioned,'' i.e., the resonance frequency at a fixed amplitude depends on the history of the specimen.

(3) When no stress is left, thermal fluctuations induce relaxation of the dynamic moduli towards an equilibrium state. As a consequence, the resonance frequency slowly returns to its initial value, with a logarithmic time recovery.

A. Behavior of a single HMU

To understand the behavior of a single HMU in dynamic conditions, we analyze the interstice response to a given applied pressure varying with time. The behavior of the interstice deformation δ has been analyzed for units representing five different classes, classified according to the relative position of P_1 and P_2 with respect to the applied pressure range. The five cases are schematized in the upper part of Fig. 5, with square brackets delimiting the pressure range. The plots of the HMU displacement δ vs pressure, time during excitation and time during relaxation are reported in the three columns for the five cases.

The following conclusions can be drawn.

(1) First column: P_1 above the maximum and P_2 above the minimum of the applied pressure range. The plot δ vs P shows no hysteretic behavior, since δ matches (with a delay) the sinusoidal behavior of the pressure. As soon as the pressure is removed, the interstice deformation vanishes.

(2) Second column: Both P_1 and P_2 are within the applied pressure range. The plot δ vs P shows a real hysteretic loop, with the appearence of a rigid state (δ independent from P) at large pressures. The sinusoidal behavior is still visible, but it cuts in the upper part due to the rigidity of the interstice. Note (particularly in the upper plot) the different pressure values at which the transitions rigid-elastic and elastic-rigid occur. Again the interstice deformation vanishes when the pressure is released, except for $P_1<0$, in which case it may remain rigid with a nonzero deformation, which returns to 0 with a random process as discussed in the next case.

(3) Third column: P_2 below the minimum and P_1 below the maximum of the applied pressure range. The plot δ vs P shows no hysteresis with a rigid interstice (except at the very beginning, if the HMU is initially in the elastic state). When the applied pressure is removed, the interstice remains deformed and eventually (if $P_2<0<P_1$) δ falls to 0, when a random transition to the elastic state occurs.

To conclude, since many HMU's follow in a chain, variations in δ in each of them may affect the pressure elsewhere as a function of time. Hence, very complex (and even chaotic) patterns may emerge, according to the location of the HMU inside the chain and its two PM space parameters P_1 and P_2.

B. Resonance frequency shift

The resonance frequency shift is analyzed in Fig. 6, where the average acceleration recorded on the free edge of the bar is plotted vs frequency for several values of the driving amplitude. In agreement with experimental results,[26] the resonance frequency ω_R is shifted downwards for increasing

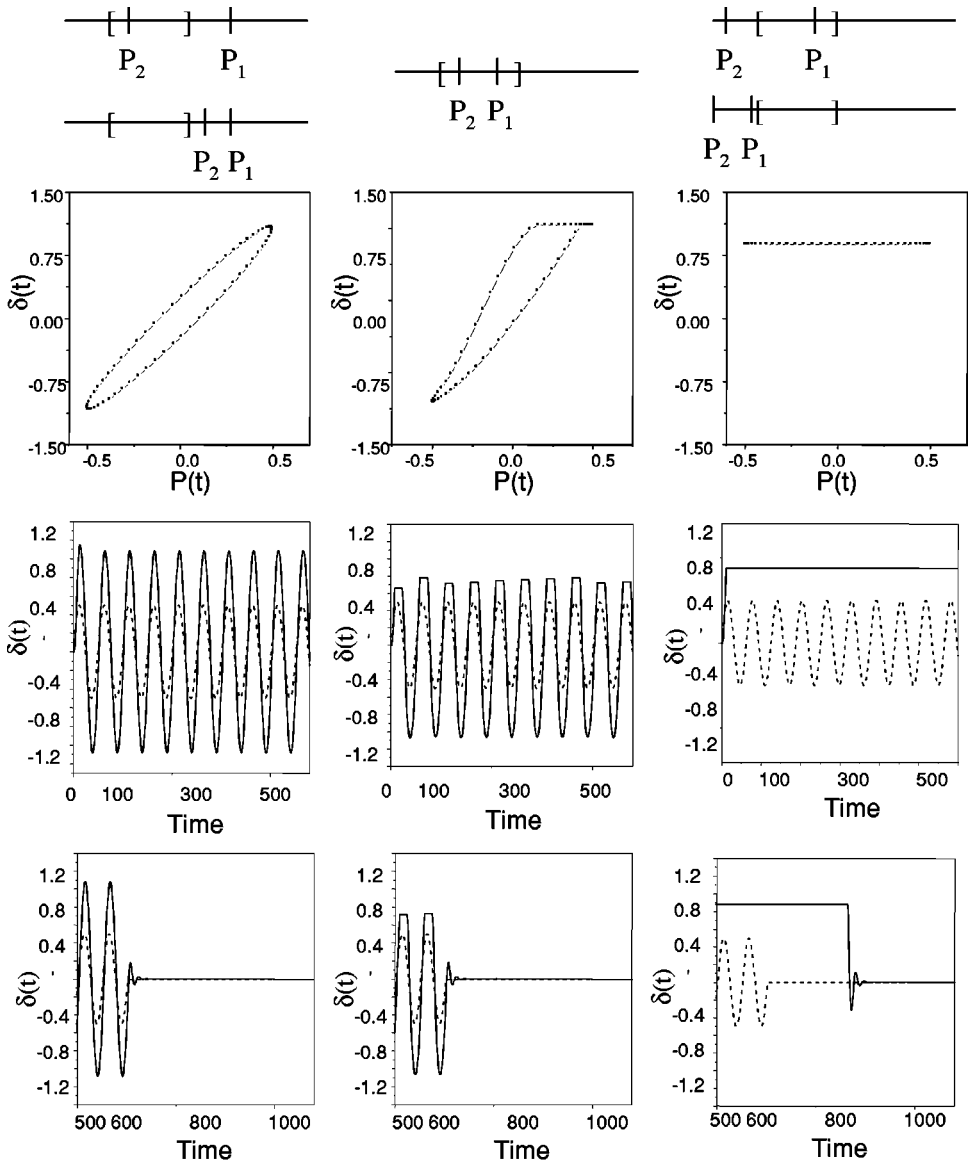

Figure 5

FIG. 5. Behavior of the interstice deformation δ for a given pressure protocol. All five different combinations of position of P_1 and P_2 with respect to the pressure range (delimited by brackets) are shown at the top of the three columns. In each column the three plots represent δ vs P, vs time during the excitation, and vs time during relaxation (from top to bottom). In the second plot the pressure is also reported as a dotted line for reference.

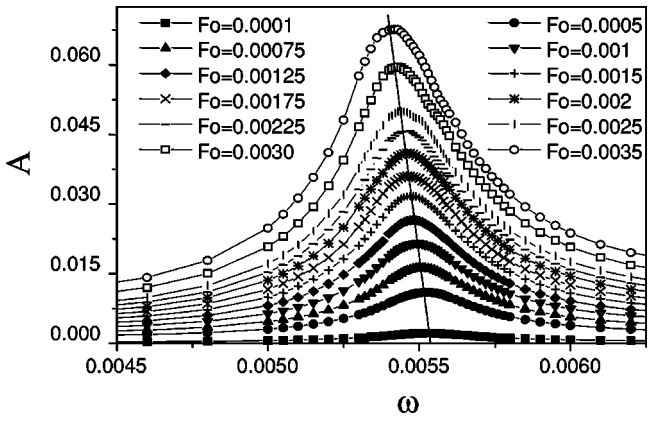

FIG. 6. Resonance frequency shift: amplitude of the received signal as a function of frequency for different values of the amplitude of the driving force F_0.

driving amplitudes. Note also a nonlinear attenuation effect due to hysteretic loops: the peak amplitude is not proportional to the driving amplitude F_0 and the width of the resonance curve becomes larger with F_0. This effect can be better appreciated in Fig. 7(b).

In Fig. 7(a) the relative frequency shift $\Delta_\omega=(\omega_R-\omega_0)/\omega_0$ is plotted vs the peak amplitude A_R in the resonance frequency curve for different values of a_2 [see Eq. (4)]. ω_0 is the "linear" resonance frequency, i.e., the limit value of the resonance frequency when the driving amplitude goes to 0. As observed experimentally,[4] Δ_ω behaves linearly with A_R, in contrast with the quadratic dependence observed in the case of classical nonlinearities. By changing the damage level of the material (e.g., the modulus of the bond, which depends on a_2), the dependence remains linear, but the slope decreases with increasing a_2.

In Fig. 7(b), to illustrate the effect of nonlinear attenuation, the quantity $\Delta_Q=(Q_R-Q_0)/Q_0$ is reported vs the peak

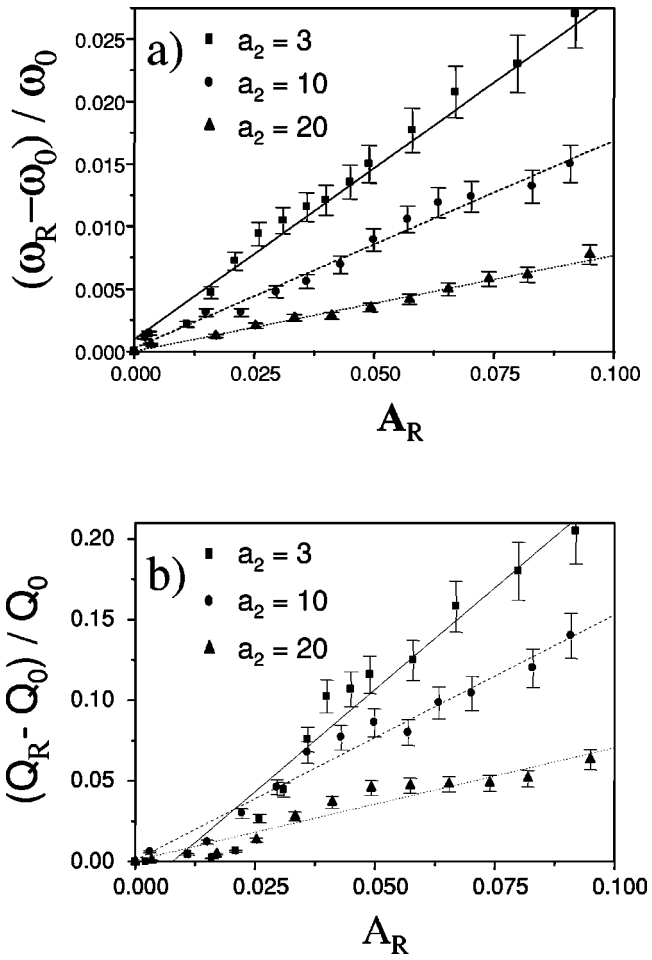

FIG. 7. Same experiment as in Fig. 6. (a) Relative frequency shift vs output amplitude at resonance, (b) Corresponding relative variation in attenuation.

amplitude A_R. Q is the quality factor and is calculated from the resonance curve by using a Lorentzian fitting. A more accurate evaluation, obtained by fitting the region close to the resonance frequency with a parabola, leads to minor corrections. Q_0 is the limit value of Q_R for $F_0 \to 0$. Again, Δ_Q is linear with the amplitude, as observed experimentally[5] for nonclassical elastic materials.

C. Conditioning

The effect of conditioning is illustrated by means of two different experiments (Figs. 8 and 9, respectively). In the first one (Fig. 8), a frequency sweep with a driving amplitude $F_0 = 0.001$ is performed, both starting with a relaxed specimen and right after prestressing with a larger driving force ($F_0 = 0.03$). The effect of the stress history in the latter case is very conspicuous both in the clear cut separation of the two curves (with two well-defined peaks) and in the higher attenuation of the latter due to the conditioning cycle. Only after a considerable amount of time does the resonance frequency of the prestressed specimen return to the ''relaxed'' value of the right peak (see the following subsection).

Another conditioning effect may be observed in Fig. 9, where we compare the resonance curves obtained by performing resonance sweeps upwards and downwards, i.e., from below to above the resonance frequency and vice versa. As observed in experimental measurements (see Fig. 1 in Ref. 11), the resonance curve is slightly different in the two cases. In fact, in the downgoing sweep the conditioning applied by the driving $A(\omega_R)$ affects measurements at frequencies lower than ω_R.

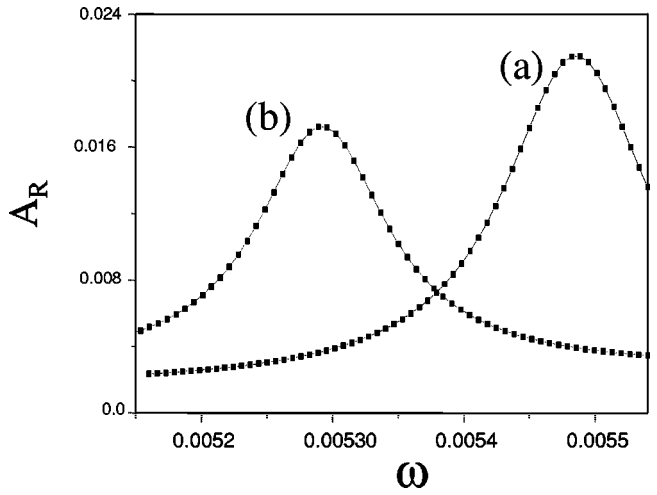

FIG. 8. First conditioning experiment: amplitude of the output signal vs frequency for a fixed forcing amplitude: (a) starting from a relaxed state, (b) after prestressing with a large amplitude driving force.

D. Recovery

An experiment of recovery (slow dynamics) is presented in Fig. 10. At first the input driving force is kept constant at a certain level F_0. Correspondingly the resonance frequency ω_R is also constant [see Fig. 10(a)]. Then, at $T = 1200\tau$, an external large amplitude disturbance F_1 is input. As a consequence, the resonance frequency drops considerably. Releasing F_1 and returning to F_0, the specimen draws back to the initial resonance frequency, with a very slow recovery, which may be monitored by a large sequence of successive resonance curve measurements. Some of them are plotted in Fig. 10(b) and show that also the attenuation is affected by the

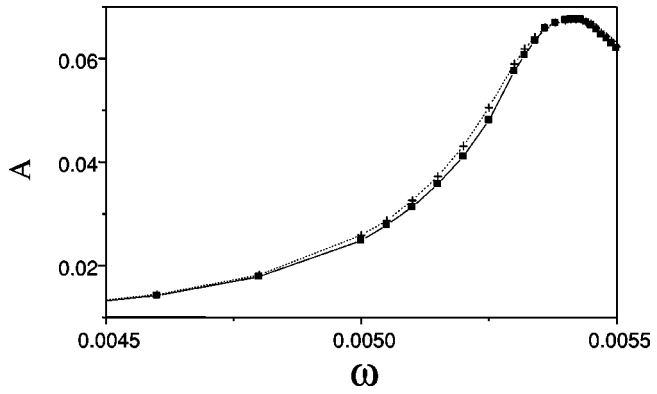

FIG. 9. Second conditioning experiment: amplitude of the output signal vs frequency in an upward (solid line with squares) and a downward (dashed line with crosses) frequency sweep.

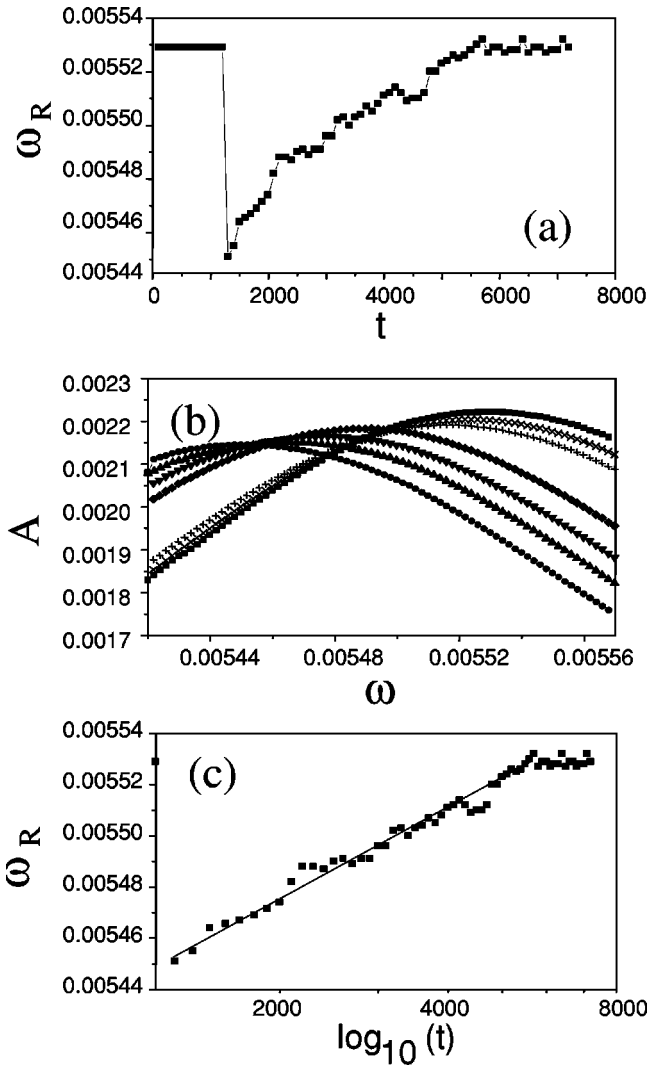

FIG. 10. Slow dynamics experiment: (a) resonance frequency vs time for a driving force fixed at a low value F_0 except for a sudden jump to a very large excitation for a very short time at $t=1200\tau$, (b) resonance curves measured at successive times during the relaxation process, (c) same as (a) but in a log(t) scale for $t>1200\tau$.

recovery process. The recovery time is extremely large, compared to typical cycling periods during resonant dynamics experiments. In Fig. 10(c), the recovery is plotted vs log(t): the resulting curve is well fitted by a straight line for a very long time interval (up to about 6000τ). Also this kind of behavior has been experimentally observed.[5]

V. CONCLUSIONS

The propagation of a monochromatic ultrasonic wave (or pulse) in a multigrained material specimen is a problem of both practical relevance (e.g., for nondestructive evaluation (NDE) purposes or in seismic studies) and theoretical interest. In fact, a rich phenomenology of both classical and nonclassical nonlinear effects has been observed and it is very enticing to look for the microscopic interaction mechanisms behind. Detailed microscopic calculations are, however, extremely difficult and the computational load required is expected to be well beyond our current possibilities.

In the present contribution a model has been proposed, which allows us to perform simulations of the ultrasonic wave propagation in multigrained aggregates, based on a simple but very supple protocol for the intersticial forces vs the local value of pressure. The implementation of the model (and selected protocol) has allowed us to obtain all the nonclassical nonlinear effects, which have been observed in resonant dynamic experiments, with an excellent qualitative agreement with the experimental data. In fact, in addition to the ''fast dynamics'' effects (such as the wave shape distortion, resonance frequency shift, and nonclassical attenuation), already explained by previous simulation approaches, the hitherto unexplained effects of conditioning and slow dynamics have been well reproduced in our simulations. This result is due to the introduction in the model of thermally activated random transition mechanisms, which have already been succesfully included in the simulation of quasistatic experiments.[14]

Although in the present context only a phenomenological protocol has been implemented, the flexibility of the model allows one to extend its applicability to all kinds of interaction mechanisms, as suggested by basic physical considerations. Work in this direction is in progress.

ACKNOWLEDGMENTS

The authors wish to thank Dr. P. A. Johnson (Los Alamos National Lab, NM) and Professor K. E.-A. Van den Abeele (Katholic University, Leuven, Belgium) for fruitful discussions. The work was supported by MURST (Grant No. MM02328989). The authors also acknowledge the support of the European Science Foundation (NATEMIS Programme).

[1] F. Cleri, S. Yip, D. Wolf, and S.R. Phillpot, Phys. Rev. Lett. **79**, 1309 (1999).
[2] I.Y. Smolin *et al.*, Comput. Mater. Sci. **19**, 133 (2000).
[3] P. Van, C. Papenfuss, and W. Muschik, Phys. Rev. E **62**, 6206 (2000).
[4] R.A. Guyer and P.A. Johnson, Phys. Today **52**, 30 (1999).
[5] R.A. Guyer, J.A. Tencate, and P.A. Johnson, Phys. Rev. Lett. **82**, 3280 (1999).
[6] J.A. TenCate, K.E-A. VanDenAbeele, T.J. Shankland, and P.A. Johnson, J. Acoust. Soc. Am. **99**, 3334 (1996).
[7] K.E.-A. VanDenAbeele, P.A. Johnson, R.A. Guyer, and K.R. McCall, J. Acoust. Soc. Am. **101**, 1885 (1997).
[8] L.D. Landau and E.M. Lifshitz, *Theory of Elasticity* (Pergamon, Oxford, 1986).
[9] R.A. Guyer, K.R. McCall, and G.N. Boitnott, Phys. Rev. Lett. **74**, 3491 (1995).

[10] J.A. TenCate and T.J. Shankland, Geophys. Res. Lett. **23**, 3019 (1996).
[11] J.A. TenCate, E. Smith, and R.A. Guyer, Phys. Rev. Lett. **85**, 1020 (2000).
[12] P.A. Johnson, in 17^{th} *ICA Proceedings, Rome, 2001*, edited by A. Alippi *et al.*, CD ROM.
[13] E. Ruffino and M. Scalerandi, Nuovo Cimento Soc. Ital. Fis., B **115**, 645 (2000).
[14] M. Scalerandi, P.P. Delsanto, and P.A. Johnson, J. Phys. D **36**, 288 (2003).
[15] M. Scalerandi, E. Ruffino, P.P. Delsanto, P.A. Johnson, and K. Van Den Abeele, in *Review of Progress in Quantitative Nondestructive Evaluation*, edited by D. O. Thompson and D.E. Chimenti, AIP Conf. Proc. No. 509 (AIP, Melville, NY, 2000), pp. 1393–99; P.P. Delsanto, V. Agostini, M. Scalerandi, and P.A. Johnson, *Phenomenology and Modeling of Damaged Mesoscopic Materials*, Proc. Conf. Euromech 419 (Prague).
[16] M. Scalerandi, V. Agostini, P.P. Delsanto, K. Van Den Abeele, and P.A. Johnson, J. Acoust. Soc. Am. **113**, 3049 (2003).
[17] R.S. Schechter, H.H. Chaskelis, R.B. Mignogna, and P.P. Delsanto, Science **265**, 1188 (1994); P. P. Delsanto, R. Mignogna, M. Scalerandi, and R. Schechter, in *New Perspectives on Problems in Classical and Quantum Physics*, edited by P.P. Delsanto and A.W. Saenz (Gordon & Breach, New Delhi, 1998), Vol. 2, pp. 51–74.
[18] P.P. Delsanto and M. Scalerandi, J. Acoust. Soc. Am. **104**, 2584 (1998).
[19] D.J. Holcomb, J. Geophys. Res. B **86**, 6235 (1981).
[20] K.R. McCall and R.A. Guyer, Non Linear Processes Geophys. **3**, 89 (1996).
[21] M. Scalerandi and V. Agostini, J. Comput. Acoust. **10**, 275 (2002).
[22] G. Gremaud and S. Kustov, Phys. Rev. B **60**, 9353 (1999); E. Nadgornyi, Prog. Mater. Sci. **31**, 210 (1988); J. Baur and W. Benoit, J. Appl. Phys. **60**, 3473 (1986).
[23] A. Aknine, B. Castagnede, and C. Depollier, C.R. Acad. Sci., Ser. IIb: Mec., Phys., Chim., Astron. **324**, 501 (1997); R. Steck *et al.*, Med. Eng. Phys. **22**, 117 (2000).
[24] X. Xia and P.G. Wolynes, Phys. Rev. Lett. **86**, 5526 (2001); V. Lunchenko and P.G. Woylnes, *ibid.* **87**, 195901 (2001).
[25] R.A. Guyer, K.R. McCall, G.N. Boitnott, L.B. Hilbert, and T.J. Plona, J. Geophys. Res., [Atmos.] **102**, 5281 (1997).
[26] P.A. Johnson, B. Zinszner, and P.N.J. Rasolofosaon, J. Geophys. Res., [Atmos.] **101**, 11553 (1996).